POTENTIALS AND LIMITATIONS OF INTEGRA® FLOWABLE WOUND MATRIX SEEDED WITH ADIPOSE TISSUE-DERIVED MICROVASCULAR FRAGMENTS

T. Später[1], F.S. Frueh[1,2], M.D. Menger[1] and M.W. Laschke[1,*]

[1] Institute for Clinical and Experimental Surgery, Saarland University, 66421 Homburg/Saar, Germany
[2] Division of Plastic Surgery and Hand Surgery, University Hospital Zurich, 8091 Zurich, Switzerland

Abstract

Adipose tissue-derived microvascular fragments (ad-MVF) represent promising vascularisation units for bioengineered Integra® matrix wound dressing (MWD). However, due to the sheet-like structure with small pore sizes, the seeding of this matrix with ad-MVF is mainly limited to its surface. Integra® flowable wound matrix (FWM) may be suitable to achieve a more homogeneous distribution and, thus, improved vascularisation, because this gel-like matrix allows for the direct admixture of ad-MVF during sample preparation. To test this hypothesis, we seeded MWD and FWM with an identical number of ad-MVF and assessed their distribution and inter-fragment distance within both matrices. Moreover, ad-MVF-seeded MWD and FWM were implanted into full-thickness skin defects within mouse dorsal skinfold chambers to analyse their vascularisation, epithelialisation and tissue incorporation using intravital fluorescence microscopy, histology and immunohistochemistry. Seeded FWM exhibited a more homogeneous ad-MVF distribution, when compared to MWD. This resulted in a significantly increased inter-fragment distance, preventing the reassembly of ad-MVF into new microvascular networks. Accordingly, the vascularisation of FWM was diminished after implantation, as indicated by a reduced functional microvessel density and blood perfusion. This was associated with a decreased tissue incorporation and epithelialisation of the matrix, when compared to ad-MVF-seeded MWD. Hence, the use of FWM as a carrier system may require a tremendous amount of ad-MVF to shorten their inter-fragment distance and, thus, to maintain their vascularisation capacity for tissue engineering applications.

Keywords: Integra®, flowable matrix, dermal substitute, skin, tissue engineering, wound healing, epithelialisation, vascularisation, dorsal skinfold chamber.

*Address for correspondence:
Matthias W. Laschke, M.D., PhD
Institute for Clinical and Experimental Surgery
Saarland University
66421 Homburg/Saar
Germany

Telephone: +49 68411626554
Fax number: +49 68411626553
Email: matthias.laschke@uks.eu

Introduction

Autologous split-thickness skin grafting represents the gold standard for skin replacement in case of extensive defects (MacNeil, 2007). For this purpose, several bioengineered matrices have been developed as off-the-shelf dermal skin substitutes, such as Integra®, Matriderm® or Glyaderm® (Pirayesh *et al.*, 2014; Shahrokhi *et al.*, 2014). In the initial phase of treatment, these matrices are directly implanted into the debrided wound bed, where they provide the required porous structure to allow cellular and vascular ingrowth from the surrounding tissue until the final coverage with split-thickness skin (Debels *et al.*, 2015). The kinetics of this biological incorporation process crucially determines the risk of wound infection, which is elevated as long as the physiological skin barrier function is not fully re-established at the defect site (Ruszczak, 2003).

Recently, we demonstrated that the seeding of Integra® matrix wound dressing (MWD) with adipose tissue-derived microvascular fragments (ad-MVF) markedly improves its epithelialisation, vascularisation and incorporation into the host tissue (Frueh *et al.*, 2017). MWD is a clinically well-established dermal skin substitute, consisting of cross-linked bovine tendon collagen and shark glycosaminoglycan (Burke *et al.*, 1981; Reid *et al.*, 2007; Graham *et al.*, 2013; Rowan *et al.*, 2015). Of interest, the seeding of the matrix with ad-MVF was mainly restricted to its surface, because larger ad-MVF could not penetrate its small pores (Frueh *et al.*, 2017). Accordingly, in the present study, we hypothesised that the seeding of ad-MVF on a dermal matrix allowing a more homogeneous distribution may result in a faster vascularisation and incorporation, when compared to MWD.

Such a matrix may be Integra® flowable wound matrix (FWM), an injectable dermal substitute of identical composition to MWD, which has been particularly developed for the treatment of complex wounds with irregular geometries (Campitiello *et al.*, 2015; Hirche *et al.*, 2016). Both MWD and FWM exhibit a comparable *in vivo* biocompatibility and vascularisation (Später *et al.*, 2016). In contrast to MWD, FWM is delivered as a granular compound that, prior to its use, needs to be hydrated with sterile saline to obtain a gel-like consistency (Campitiello *et al.*, 2015). Therefore, we further hypothesised that this sample preparation would allow a more homogeneous admixture of ad-MVF into FWM.

To test our hypotheses, we seeded MWD and FWM with an identical number of ad-MVF and assessed their distribution and inter-fragment distance within both matrices. In addition, the ad-MVF-seeded matrices were implanted into full-thickness skin defects within mouse

dorsal skinfold chambers to analyse their vascularisation, epithelialisation and tissue incorporation throughout an observation period of 14 d by means of repetitive intravital fluorescence microscopy, histology and immunohistochemistry.

Materials and Methods

Animals

All animal experiments were approved by the local governmental animal care committee (permit number: 08/2015) and conducted in accordance with the European legislation on the protection of animals (Directive 2010/63/EU) and the NIH guidelines on the care and use of laboratory animals (NIH publication #85-23 Rev. 1985).

Dorsal skinfold chambers were implanted in wild-type C57BL/6 mice (Institute for Clinical and Experimental Surgery, Saarland University, Homburg, Germany) with an age of 4-6 months and a body weight of 24-28 g. Epididymal fat was isolated from male green fluorescent protein (GFP)+ mice [C57BL/6-Tg(CAG-EGFP)1Osb/J; The Jackson Laboratory, Bar Harbor, ME, USA] with an age of 12-18 months and a body weight of ≥ 30 g, to guarantee large epididymal fat pads containing sufficient amounts of ad-MVF for the seeding of the matrices (Grässer *et al.*, 2016). The animals were housed under a 12 h light/dark cycle and were fed *ad libitum* with water and standard food pellets (Altromin, Lage, Germany).

Isolation of ad-MVF

As previously described in detail, ad-MVF were isolated from epididymal fat pads of GFP+ donor mice (Frueh *et al.*, 2017). Briefly, the bilateral epididymal fat pads were removed, transferred into 10 % Dulbecco's modified eagle medium (DMEM; 100 U/mL penicillin, 0.1 mg/mL streptomycin; Biochrom, Berlin, Germany) and washed thrice with phosphate-buffered saline (PBS). Then, the isolated fat tissue was minced and digested for 10 min with collagenase NB4G (0.5 U/mL; Serva, Heidelberg, Germany) under slow stirring and humidified atmospheric conditions (37 °C, 5 % CO_2). Subsequently, the digestion was neutralised with PBS supplemented with 20 % foetal calf serum (FCS) and the cell-vessel suspension was incubated for 5 min at 37 °C. Next, the fat supernatant was removed and the remaining cell-vessel suspension was filtered through a 500 µm mesh. The GFP+ ad-MVF were enriched up to a pellet size by a 5 min centrifugation at 120 ×*g*. Before that, the ad-MVF were seeded on MWD and FWM, the remaining cell-vessel pellet was resuspended in 15 µL 0.9 % NaCl.

Seeding of MWD and FWM

MWD samples were identically cut out of a 1.3 mm thick Integra® dermal regeneration template single layer without silicone sheet (Integra Life Sciences, Ratingen, Germany), using a 4 mm biopsy punch (Kai Medical, kaiEurope GmbH, Solingen, Germany). Each MWD sample was placed on a 500 µm cell strainer and 15 µL 0.9 % NaCl containing ~15,000 ad-MVF were transferred onto the implant with a 20 µL pipette (Eppendorf, Wesseling-Berzdorf, Germany).

To generate an ad-MVF-seeded FWM sample, 1.25 mg of the granulated collagen-glycosaminoglycan were carefully hydrated with 15 µL of 0.9 % NaCl containing an identical number of ad-MVF.

Modified dorsal skinfold chamber model

For the *in vivo* analysis of the ad-MVF-seeded matrices, we used a modified dorsal skinfold chamber model according to Sorg *et al.* (2007; 2009). For the implantation of the dorsal skinfold chamber (Irola Industriekomponenten GmbH & Co. KG, Schonach, Germany), the mice were anaesthetised by intraperitoneal injection of ketamine (75 mg/kg body weight; Ursotamin®; Serumwerke Bernburg, Bernburg, Germany) and xylazine (25 mg/kg body weight; Rompun®, Bayer, Leverkusen, Germany). Then, two symmetrical titanium frames were implanted on the extended dorsal skinfold, as described previously in detail (Laschke and Menger, 2016). After a recovery period of 2 d, the mice were anaesthetised again to create a 4 mm full-thickness skin defect within the observation window of the chamber by means of a dermal biopsy punch (Kai Medical) and microsurgical instruments. After the defect was filled with either an ad-MVF-seeded MWD sample or an identical volume of ad-MVF-seeded FWM, the observation window of the chamber was sealed with a removable cover glass.

Stereomicroscopy

To assess the epithelialisation of both ad-MVF-seeded MWD and FWM by planimetry, the anaesthetised animals were fixed on a Plexiglas® stage and the dorsal skinfold chamber was positioned under a stereomicroscope (Leica M651, Wetzlar, Germany) on day 0 (day of implantation) as well as day 3, 6, 10 and 14. The chamber tissue was visualised in epi-illumination to identify epithelialised and non-epithelialised areas. The microscopic images were recorded by a DVD system and quantitatively analysed using the CapImage computer-assisted off-line analysis system (Zeintl, Heidelberg, Germany). The epithelialised area (given in %) was calculated by the equation: (Total implant area − non-epithelialised implant area)/total implant area × 100.

Intravital fluorescence microscopy

After stereomicroscopy, 0.1 mL of the blood plasma marker 5 % FITC-labelled dextran (150,000 Da; Sigma-Aldrich, Taufkirchen, Germany) was injected in the retrobulbar venous plexus of the anaesthetised animals for contrast enhancement. The observation window of the chamber was positioned under a Zeiss Axiotech microscope (Zeiss, Oberkochen, Germany) and the microscopic images were recorded by a charge-coupled device video camera (FK6990; Pieper, Schwerte, Germany) and a DVD system for off-line analysis (Laschke *et al.*, 2015).

The analysis of the microscopic images was performed using CapImage (Zeintl). Vascularisation of the implants' surface was assessed in 12 regions of interest (ROIs). ROIs exhibiting red blood cell (RBC)-perfused microvessels were defined and counted as perfused ROIs (in % of all ROIs). The functional microvessel density was determined as the length of all RBC-perfused microvessels per area of

the ROI (cm/cm^2). Moreover, both diameter (d, in µm) and centreline RBC velocity (v, µm/s) of 40 randomly selected microvessels were measured. These two parameters were then used to calculate the wall shear rate (y, in s^{-1}) by means of the Newtonian definition y = 8 × v/d (Ampofo *et al.*, 2016).

Experimental protocol

In a first set of experiments, ad-MVF were harvested from 3 GFP$^+$ donor mice. Half of the ad-MVF were seeded onto 3 MWD samples, while the other half was admixed in 3 FWM samples. Directly after seeding, the samples were processed for the histological analysis of the distribution and distance of ad-MVF within the matrices.

For the *in vivo* analyses, ad-MVF were harvested from 11 male GFP$^+$ donor mice. Half of the ad-MVF were seeded on 11 MWD samples, while the other half was admixed in 11 FWM samples. Both MWD and FWM samples were implanted into full-thickness skin defects in dorsal skinfold chambers of 22 wild-type C57BL/6 mice. Vascularisation and epithelialisation of 8 implants per group were analysed by means of stereomicroscopy and intravital fluorescence microscopy on day 0 (day of implantation), 3, 6, 10 and 14. Thereafter, the animals were sacrificed with an overdose of anaesthesia and the dorsal skinfold chamber preparations were processed for histological and immunohistochemical analyses. For additional immunohistochemical analyses at an earlier time point, 3 animals per group were already sacrificed on day 6 after implantation.

Histology and immunohistochemistry

Formalin-fixed specimens of freshly ad-MVF-seeded MWD and FWM samples, as well as dorsal skinfold preparations with their implants, were embedded in paraffin and cut into 3 µm thick sections. Haematoxylin and eosin (HE) staining of individual sections was performed
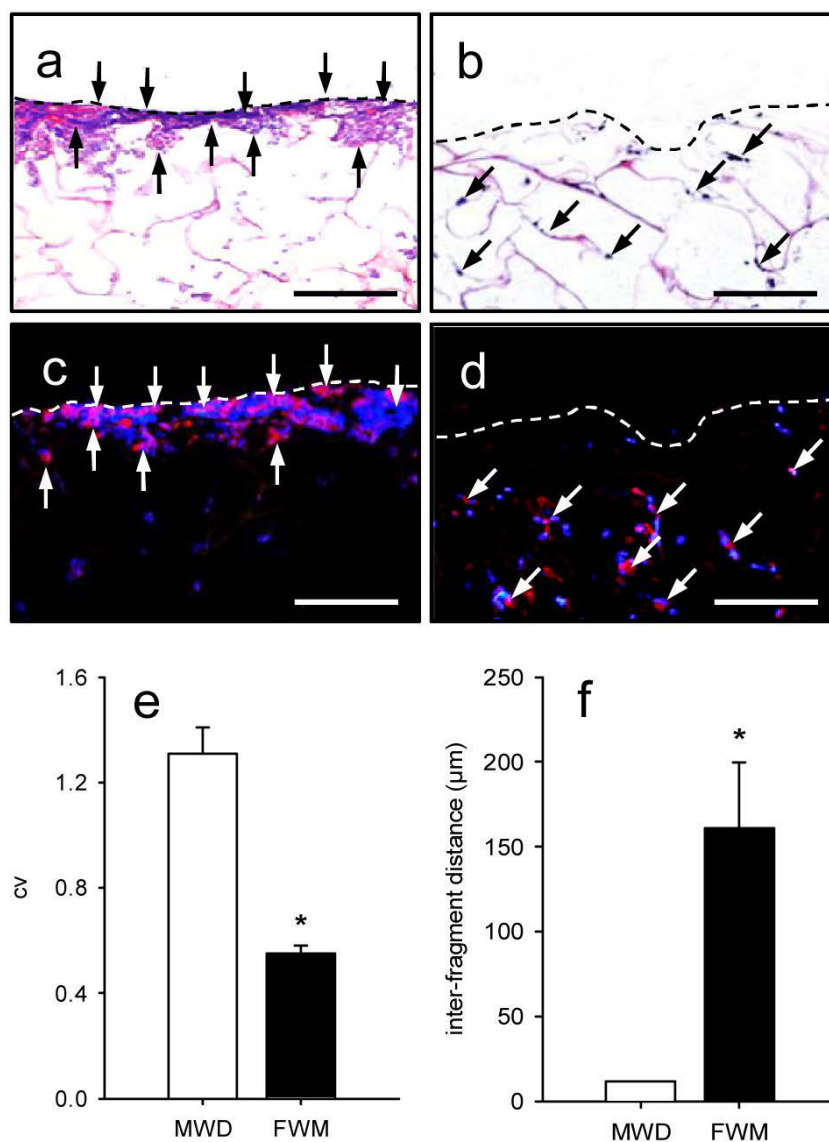
**Fig. 1.** HE-stained and immunofluorescent sections of (**a**, **c**) ad-MVF-seeded MWD and (**b**,**d**) FWM immediately after seeding (broken line = implant border; arrows = ad-MVF). The immunofluorescent sections were stained with an antibody against CD31 to detect blood vessels (**c**,**d**, red) and Hoechst 33342 to detect cell nuclei (**c**,**d**, blue). Scale bars= 100 µm. (**e**) cv and (**f**) inter-fragment distance of ad-MVF-seeded MWD (white bars; *n* = 3) and FWM (black bars; *n* = 3). Mean ± SEM. * *p* < 0.05 *vs.* MWD.

according to standard procedures. To quantify the collagen content of implanted MWD and FWM, additional sections were stained with sirius red. Using a BX60 microscope (Olympus, Hamburg, Germany) and the imaging software cellSens Dimension 1.11 (Olympus), the collagen content was assessed in relation to normal skin in 4 ROIs per sample (Frueh *et al.*, 2017).

Freshly ad-MVF-seeded MWD and FWM were embedded in Tissue-tek® O.C.T. compound (A. Hartenstein GmbH, Würzburg, Germany), quickly-frozen in liquid nitrogen at −196 °C and subsequently cut into 3 µm thick cryosections. The sections were stained with a monoclonal rat anti-mouse antibody against the endothelial cell marker CD31 (1 : 100; Dianova, Hamburg, Germany). A goat anti-rat IgG Alexa555 antibody (Life Technologies, Eugene, OR, USA) served as secondary antibody. Cell nuclei were stained with Hoechst 33342 (1 : 500; Sigma-Aldrich). The sections were examined with a BX60 microscope
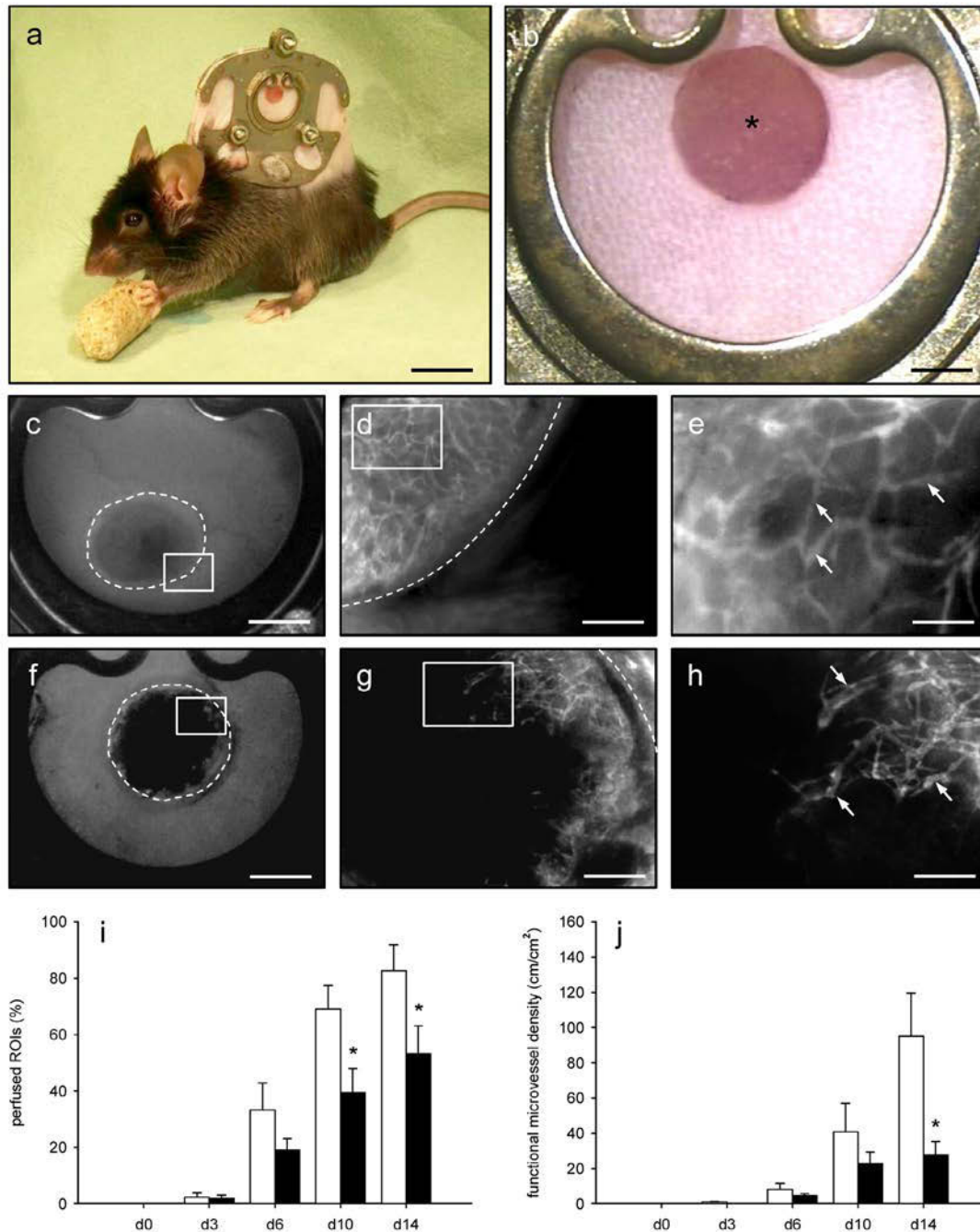
Fig. 2. (**a**) C57BL/6 mouse with a dorsal skinfold chamber. Scale bar = 13 mm. (**b**) Overview of the chamber observation window with an ad-MVF-seeded MWD implant in a 4 mm full-thickness skin defect (asterisk). Scale bar = 1.5 mm. Intravital fluorescence microscopy (blue light epi-illumination with 5 % FITC-labelled dextran 150,000 i.v.) of implanted (**c-e**) ad-MVF-seeded MWD and (**f-h**) FWM on day 14 (broken line = implant border; **d,g** = insert in **c** and **f**; **e,h** = insert in **d** and **g**; arrows = perfused microvessels). Scale bars: **c,f** = 2 mm; **d,g** = 400 µm; **e,h** = 100 µm. (**i**) Perfused ROIs and (**j**) functional microvessel density of ad-MVF-seeded MWD (white bars; *n* = 8) and FWM (black bars; *n* = 8). Mean ± SEM. * *p* < 0.05 *vs.* MWD.

(Olympus) to assess the distribution and the distance of individual ad-MVF within the samples. For this purpose, the number of CD31$^+$ microvessels was determined in 20 ROIs per implant (equivalent to the entire implant area per section), to calculate the coefficient of variation (cv; standard deviation/mean) of the spatial fragment distribution. Moreover, the inter-fragment distance (given in µm) was measured in 5 randomly selected ROIs.

In addition, dorsal skinfold preparations with their implants were co-stained using a monoclonal rat anti-mouse antibody against the endothelial cell marker CD31 (1 : 100; Dianova) and a polyclonal goat antibody against GFP (1 : 200; Rockland immunochemicals, Limerick, ME, USA). A goat anti-rat IgG Alexa555 antibody (Life Technologies) and a biotinylated donkey anti-goat antibody (1 : 30; Dianova) served as secondary antibodies. The biotinylated antibody was detected by streptavidin-Alexa488 (1 : 50; Life Technologies). Cell nuclei were stained with Hoechst 33342 (1 : 500; Sigma-Aldrich). Quantitative analyses of the sections included the determination of the density of CD31$^+$ microvessels (given in mm^{-2}) and the fraction of CD31$^+$/GFP$^+$ microvessels (given in %) within the implants.

For the detection of cleaved caspase-3$^+$ and Ki67$^+$ cells, sections were incubated with a rabbit polyclonal anti-cleaved caspase-3 antibody (1 : 100; New England Biolabs, Frankfurt, Germany) or a rabbit polyclonal anti-Ki67 antibody (1 : 500; Abcam, Cambridge, UK) as primary antibody, followed by a biotinylated goat anti-rabbit IgG antibody (ready-to-use; Abcam) as secondary antibody. The biotinylated antibody was detected by peroxidase-labelled-streptavidin (1 : 50; Sigma-Aldrich). 3-Amino-9-ethylcarbazole (Abcam) was used as chromogen. The sections were counterstained with Mayer's haemalum (Merck, Darmstadt, Germany). Quantitative analyses of the sections included the determination of the fractions of cleaved caspase-3$^+$ and Ki67$^+$ cells (given in %) in 6 randomly selected ROIs within the implants on day 6 and 14.

On day 14, for the immunohistochemical detection of the cytokeratin$^+$ epithelial layers covering the implants, sections of the largest cross-sectional diameter of the matrices were incubated with a rabbit polyclonal anti-cytokeratin antibody (1 : 100; Abcam) as primary antibody, followed by a biotinylated goat anti-rabbit IgG antibody (ready-to-use; Abcam). The biotinylated antibody was detected by peroxidase-labelled-streptavidin (1 : 50; Sigma-Aldrich). 3,3-Diaminobenzidine (Sigma-Aldrich) was used as chromogen. Using a BZ-8000 microscopic system (Keyence, Osaka, Japan), the length of the cytokeratin$^+$ epithelial layer and the diameter of the implants were measured to assess epithelialisation as follows:

(Length of cytokeratin$^+$ epithelial layer/total diameter of implant) $\times$ 100.

Statistical analysis

After testing the data for normal distribution and equal variance, differences between the groups were analysed by the unpaired Student's *t*-test (SigmaStat; Jandel Corporation, San Rafael, CA, USA). All values were expressed as means ± SEM. Statistical significance was accepted for a value of $p < 0.05$.

## Results

Ad-MVF distribution within seeded implants

The examination of HE-stained histological sections of freshly seeded MWD and FWM showed that ad-MVF were almost exclusively localised on the surface of MWD (Fig. 1**a**), whereas FWM exhibited a more homogeneous distribution of the microvessels (Fig. 1**b**). These observations were confirmed by quantitative analyses of CD31-stained sections of the matrices. The analyses revealed a significantly lower cv for the spatial fragment distribution within FWM, when compared to MWD (Fig. 1**c**-**e**). Because both matrices were seeded with ~15,000 ad-MVF, the more homogeneous distribution within FWM also resulted in a ~15 fold higher inter-fragment distance (Fig. 1**f**).

Vascularisation and incorporation of the implants

To analyse the vascularisation of ad-MVF-seeded MWD and FWM we used a modified mouse dorsal skinfold chamber model (Fig. 2**a**,**b**). This model allowed repetitive

Table 1. Diameter, centreline RBC velocity and wall shear rate of the microvasculature within ad-MVF-seeded MWD (*n* = 8) and FWM (*n* = 8) directly (0 d) as well as 3, 6, 10 and 14 d after implantation into dorsal skinfold chambers. Mean ± SEM. * $p < 0.05$ *vs.* MWD.

|	0 d	3 d	6 d	10 d	14 d
Diameter [µm]:					
MWD	-	27.5 ± 8.6	27.4 ± 2.6	22.3 ± 2.7	18.1 ± 1.5
FWM	-	23.3 ± 5.2	32.9 ± 5.4	16.8 ± 0.8*	14.7 ± 0.9
Centreline RBC velocity [µm/s]:					
MWD	-	150.6 ± 65.9	428.9 ± 111.8	696.4 ± 66.0	643.3 ± 79.2
FWM	-	62.5 ± 35.5	101.1 ± 37.6	420.3 ± 89.7	461.9 ± 60.7
Wall shear rate [s^{-1}]:					
MWD	-	59.6 ± 21.5	136.4 ± 42.7	268.7 ± 37.4	292.9 ± 51.6
FWM	-	19.7 ± 7.8	25.8 ± 11.2*	203.3 ± 44.4	250.5 ± 24.3
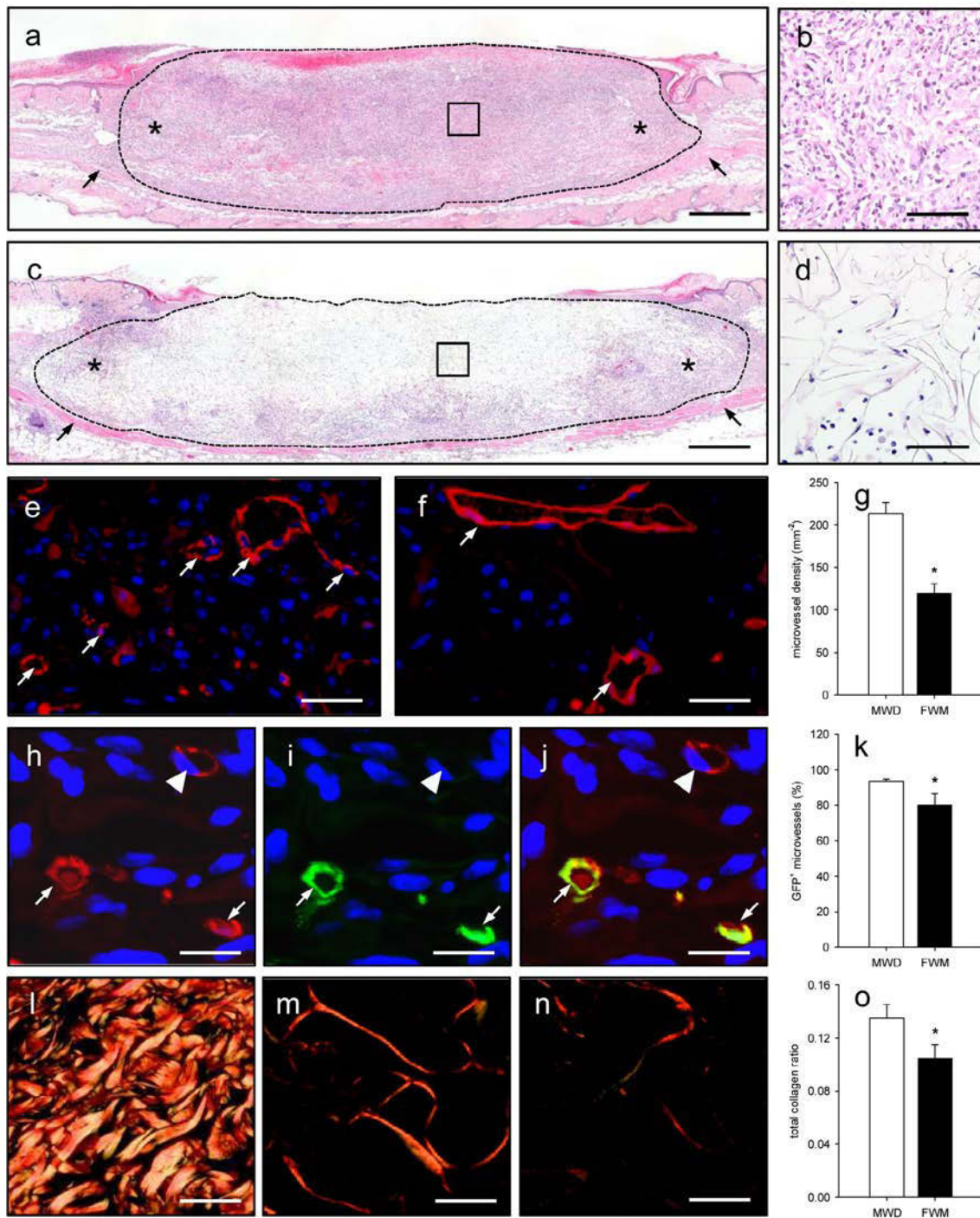
Fig. 3. HE-stained sections of (**a,b**) ad-MVF-seeded MWD and (**c,d**) FWM on day 14 (broken line = implant border; asterisks = border zones; arrows = panniculus carnosus muscle of the dorsal skinfold chamber preparation; **b,d** = insert in **a** and **c**). Scale bars: **a,c** = 350 µm; **b,d** = 50 µm. (**e,f**) Immunohistochemical detection of CD31$^+$ (red) microvessels (arrows) in (**e**) ad-MVF-seeded MWD and(**f**) FWM on day 14. Scale bars = 30 µm. (**g**) Microvessel density of ad-MVF-seeded MWD (white bar; $n = 8$) and FWM (black bar; $n = 8$). (**h-j**) Immunohistochemical detection of microvessels in an ad-MVF-seeded FWM (arrows = CD31$^+$ (red)/GFP$^+$ (green) microvessels; arrowhead = CD31$^+$/GFP$^-$ microvessel; **j** = merge of **h** and **i**). Scale bars = 15 µm. (**k**) GFP$^+$ microvessels in ad-MVF-seeded MWD (white bar; $n = 8$) and FWM (black bar; $n = 8$). (**l-n**) Polarised light microscopy of sirius red stained sections of (**l**) normal skin, (**m**) ad-MVF-seeded MWD and (**n**) FWM. Scale bars = 125 µm. (**o**) Total collagen ratio (implant/skin) of ad-MVF-seeded MWD (white bar; $n = 8$) and FWM (black bar; $n = 8$). Mean ± SEM. * $p < 0.05$ *vs.* MWD.

intravital fluorescent microscopic analyses of the implants' surface in full-thickness skin defects throughout an observation period of 14 d. Our analyses revealed that the seeded ad-MVF reassembled into new microvascular networks in both experimental groups over time. Also, at the borders of the skin defects, these networks developed interconnections to the vessels of the surrounding host microvasculature, resulting in the onset of blood perfusion. Of interest, the pace and extent of this process was markedly diminished in implanted FWM samples (Fig. 2**c-h**). Accordingly, the FWM group exhibited a significantly reduced number of perfused ROIs between day 10 and 14 and functional microvessel density on day 14, when compared to the MWD group (Fig. 2**i,j**).

Measurements of microhaemodynamic parameters showed that, over time, the diameter of blood-perfused microvessels decreased and both the centreline RBC velocity and wall shear rate increased in ad-MVF-seeded MWD and FWM (Table 1). Although not proven to be significant at each time point, the diameter, centreline RBC velocity and wall shear rate of microvessels within FWM were found to be reduced when compared to MWD (Table 1).

In addition, to assess vascularisation and cellular infiltration throughout their entire cross section, MWD and FWM implants were further examined by means of histology and immunohistochemistry at the end of the 14 d observation period. The analysis of HE-stained sections revealed that most pores of ad-MVF-seeded MWD were filled with a dense vascularised granulation tissue (Fig. 3**a,b**). In contrast, vascularisation of FWM was only observed in the border zones, while the centre of the implants only contained few single cells (Fig. 3**c,d**). Accordingly, the density of CD31^{+} microvessels was significantly reduced within FWM, when compared to MWD (Fig. 3**e-g**). More detailed CD31^{+}/GFP^{+} co-staining analyses of the microvascular networks revealed that ~93 % of all detected microvessels in MWD originated from GFP^{+} ad-MVF (Fig. 3**h-k**). This fraction was reduced to ~80 % in ad-MVF-seeded FWM (Fig. 3**k**). To further
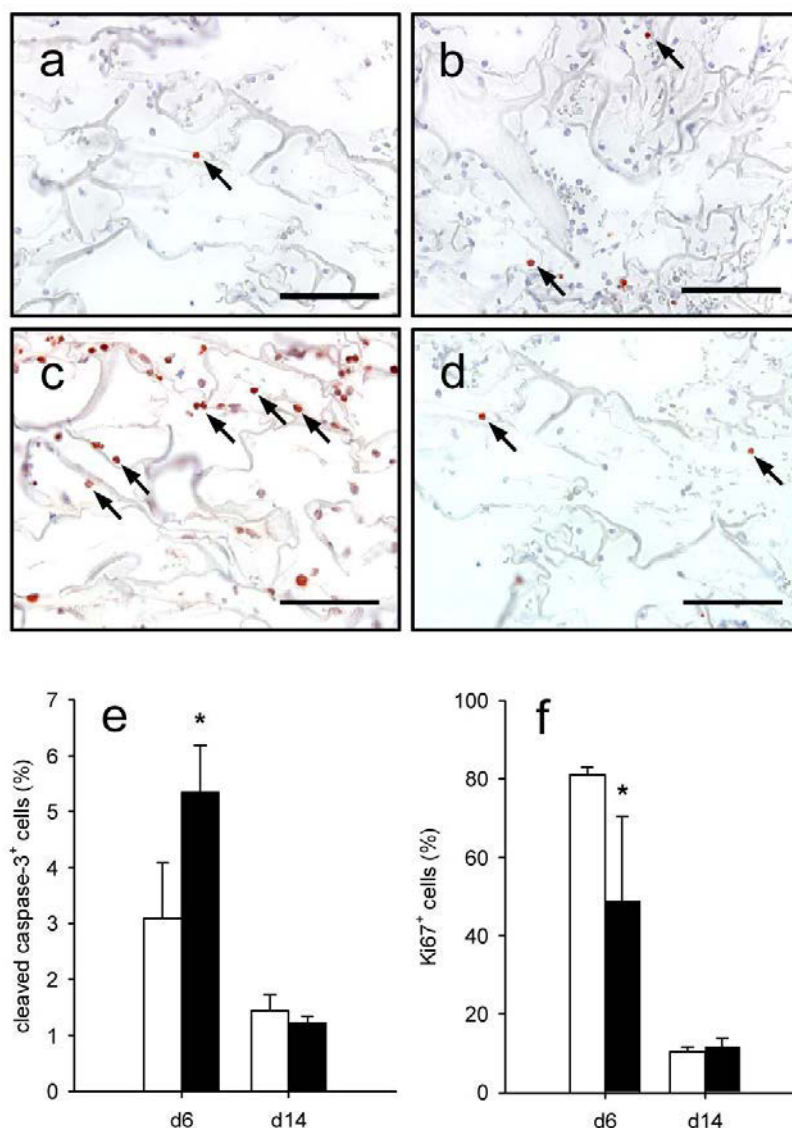
Fig. 4. Immunohistochemical detection of (**a,b**; arrows) cleaved caspase-3[+] and (**c,d**; arrows) Ki67^{+} cells in (**a,c**) ad-MVF-seeded MWD and (**b,d**) FWM on day 6. Scale bars = 50 µm. (**e**) Cleaved caspase-3[+] and (**f**) Ki67^{+} cells within ad-MVF-seeded MWD (white bars; day 6: $n = 3$, day 14: $n = 8$) and FWM (black bars; day 6: $n = 3$, day 14: $n = 8$) on day 6 and 14. Mean ± SEM. * $p < 0.05$ *vs.* MWD.

analyse the amount of collagen within the implants, a sirius red staining was used to detect mature collagen type I fibres by their reddish appearance under polarised light (Junqueira *et al.*, 1979; Radhika *et al.*, 2016). The quantitative analysis of this staining showed a significantly lower collagen ratio in FWM, when compared to MWD (Fig. 3**l**-**o**). Taken together, these results indicated a markedly reduced vascularisation and tissue incorporation of ad-MVF-seeded FWM.

Apoptotic cell death and proliferation within the implants

The immunohistochemical detection of cleaved caspase-3 and Ki67 showed that ad-MVF-seeded FWM contained a significantly higher number of apoptotic cells and reduced number of proliferating cells on day 6, when compared to MWD (Fig. 4**a**-**f**). On day 14, the matrices exhibited comparably small numbers of apoptotic and proliferating cells, without significant differences between the two groups (Fig. 4**e**,**f**).

Epithelialisation of the implants

The observation window of the dorsal skinfold chamber allowed a continuous access to the implants and,

thus, a repetitive stereomicroscopic analysis of their epithelialisation (Fig. 5**a**-**f**). This analysis revealed that the epithelialisation of ad-MVF-seeded FWM was significantly reduced between day 6 and 14, when compared to MWD (Fig. 5**g**). These findings were confirmed by additional immunohistochemical analyses of the implants on day 14, demonstrating that ~75 % of the MWD surface were covered with a cytokeratin+ epithelial layer (Fig. 5**h**,**j**). In contrast, only ~40 % of the FWM surface exhibited a cytokeratin+ epithelial coverage (Fig. 5**i**,**j**).

Discussion

Bioengineered dermal skin substitutes, such as Integra®, provide an off-the-shelf solution for the rapid treatment of extensive skin defects. A sufficient vascularisation is the major prerequisite for their final coverage with split-thickness skin grafts after 2-3 weeks (Debels *et al.*, 2015). To shorten this critical time period, which is associated with an increased risk of wound infection, the seeding of dermal substitutes with different cell types has been suggested as a promising approach to stimulate the formation of new blood vessels within the implants (Lamme *et al.*, 1998;
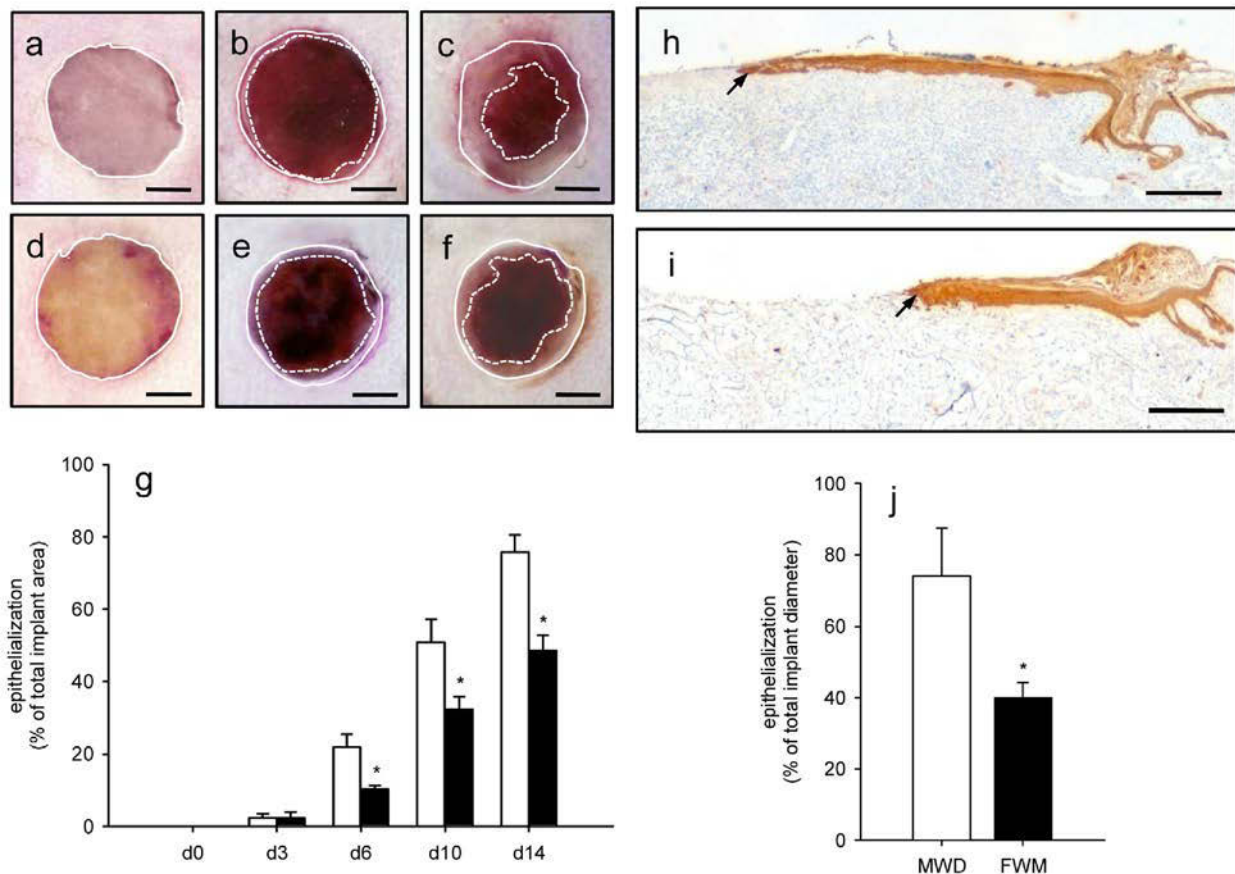
Fig. 5. Stereomicroscopic images of skin defects in dorsal skinfold chambers of C57BL/6 mice with (**a-c**) ad-MVF-seeded MWD and (**d-f**) FWM directly after implantation (**a,d**) as well as on day 6 (**b,e**) and 14 (**c,f**) (closed line = implant border; broken line = non-epithelialised area). Scale bars = 1.5 mm. (**g**) Epithelialisation (% of total implant area) of implanted ad-MVF-seeded MWD (white bars; $n = 8$) and FWM (black bars; $n = 8$). Mean ± SEM. * $p < 0.05$ *vs.* MWD. (**h,i**) Immunohistochemical detection of the cytokeratin+ epithelial layer (arrow) covering (**h**) ad-MVF-seeded MWD and (**i**) FWM on day 14 after implantation. Scale bars = 100 µm. (**j**) Epithelialisation (% of total implant diameter) of ad-MVF-seeded MWD (white bar; $n = 8$) and FWM (black bar; $n = 8$). Mean ± SEM. * $p < 0.05$ *vs.* MWD.

Young *et al.*, 1998; Melendez *et al.*, 2008; Danner *et al.*, 2012; Meruane *et al.*, 2012; Killat *et al.*, 2013; Zonari *et al.*, 2015). Recently, we could demonstrate that the seeding of dermal skin substitutes with ad-MVF, which already represent fully functional vessel segments, may be even more effective (Frueh *et al.*, 2017). Accordingly, they only need to develop interconnections with each other and the surrounding host microvasculature to get rapidly reperfused within a few days (Laschke and Menger, 2015). Moreover, ad-MVF also contain mesenchymal stem cells and endothelial progenitor cells (Laschke *et al.*, 2012; McDaniel *et al.*, 2014). These multipotent cells further contribute to their high regenerative potential.

The seeding of dermal matrices with multi-cellular components, such as ad-MVF, is challenging. In fact, these matrices typically exhibit small pore sizes (< 200 µm; Frueh *et al.*, 2016). This structure has been shown to promote the formation of microvascular networks with small-diameter vessels with high density and poor penetration depth (Choi *et al.*, 2013; Frueh *et al.* 2016). Accordingly, we herein confirmed that ad-MVF were almost exclusively localised on the surface of freshly seeded MWD, as previously shown (Frueh *et al.*, 2017). In contrast, FWM offered the major advantage that ad-MVF could be directly admixed into the matrix during the sample preparation, leading to a more homogeneous distribution. However, against our expectations, this did not result in an improved vascularisation and tissue incorporation of FWM after implantation into full-thickness skin defects.

This finding was most probably due to an increased inter-fragment distance. In fact, both MWD and FWM were seeded with a comparable number of ~15,000 ad-MVF. Therefore, the more homogeneous distribution in the FWM group was associated with a ~15-fold higher inter-fragment distance. Hence, the ad-MVF needed more time to bridge the distance between each other. In addition, the reassembly of ad-MVF into new microvascular networks has been shown to be crucially dependent on the interconnection of individual angiogenic sprouts growing out of the vessel segments (Nunes *et al.*, 2010). In contrast to FWM, the extremely high density of ad-MVF on the surface of MWD may have markedly increased the probability for this event and the inosculation of the newly developing microvascular networks to the surrounding blood vessels of the host tissue. Accordingly, the blood perfusion of ad-MVF-seeded MWD samples was accelerated and improved in the early phase after implantation, as indicated by a higher centreline RBC velocity and wall shear rate in individual microvessels. This, in turn, may have contributed to an increased survival rate of the seeded ad-MVF. In line with this view, MWD implants exhibited a reduced number of apoptotic cells on day 6 as well as an increased fraction of CD31^{+}/GFP^{+} microvessels on day 14, when compared to FWM samples. Consequently, histological and immunohistochemical analyses at the end of the 14 d observation period revealed that most pores of ad-MVF-seeded MWD were filled with a dense vascularised granulation tissue. This indicated a good incorporation of the matrix into the surrounding tissue, which was associated with an increased cellular proliferation rate and collagen content as well as an accelerated epithelialisation

over time, when compared to FWM implants. Hence, these findings demonstrated that a locally limited high seeding density of ad-MVF was already sufficient to achieve a rapid implant vascularisation.

Finally, it may be assumed that it is also possible to further improve the vascularisation of FWM by means of ad-MVF. However, for this purpose, a greater number of ad-MVF per implant would be necessary to shorten their inter-fragment distance and, thus, to maintain their ability to reassemble into new microvascular networks. In our previous study we have reported that the seeding of 1 cm² MWD already requires ~120,000 ad-MVF isolated from ~3 mL fat tissue (Frueh *et al.*, 2017). Therefore, ad-MVF-seeded FWM may be particularly recommended as an injectable ad-MVF carrier for the minimal invasive filling of small, hardly accessible defects with an irregular geometry. In contrast, for the coverage of large skin defects, such as caused by extensive burns, ad-MVF-seeded MWD may be more suitable.

Conclusions

FWM bears the major potential to allow for a more homogeneous distribution of cellular material in comparison to MWD. However, in case of seeded ad-MVF this is associated with an increased inter-fragment distance, which prevents the development of new microvascular networks. Accordingly, the use of FWM as a carrier system may require a tremendous amount of ad-MVF to maintain their vascularisation capacity for tissue engineering applications.

References

Ampofo E, Widmaier D, Montenarh M, Menger MD, Laschke MW (2016) Protein kinase CK2 regulates leukocyte-endothelial cell interactions during ischemia and reperfusion in striated skin muscle. Eur Surg Res **57**: 111-124.

Burke JF, Yannas IV, Quinby WC Jr, Bondoc CC, Jung WK (1981) Successful use of a physiologically acceptable artificial skin in the treatment of extensive burn injury. Ann Surg **194**: 413-428.

Campitiello F, Della Corte A, Guerniero R, Pellino G, Canonico S (2015) Efficacy of a new flowable wound matrix in tunneled and cavity ulcers: a preliminary report. Wounds **27**: 152-157.

Choi SW, Zhang Y, Macewan MR, Xia Y (2013) Neovascularization in biodegradable inverse opal scaffolds with uniform and precisely controlled pore sizes. Adv Healthc Mater **2**: 145-154.

Danner S, Kremer M, Petschnik AE, Nagel S, Zhang Z, Hopfner U, Reckhenrich AK, Weber C, Schenck TL,

Becker T, Kruse C, Machens HG, Egaña JT (2012) The use of human sweat gland-derived stem cells for enhancing vascularization during dermal regeneration. J Invest Dermatol **132**: 1707-1716.

Debels H, Hamdi M, Abberton K, Morrison W (2015) Dermal matrices and bioengineered skin substitutes: a critical review of current options. Plast Reconstr Surg Glob Open **3**: e284.

Frueh FS, Menger MD, Lindenblatt N, Giovanoli P, Laschke MW (2016) Current and emerging vascularization strategies in skin tissue engineering. Crit Rev Biotechnol **20**: 1-13.

Frueh FS, Später T, Lindenblatt N, Calcagni M, Giovanoli P, Scheuer C, Menger MD, Laschke MW (2017) Adipose tissue-derived microvascular fragments improve vascularization, lymphangiogenesis, and integration of dermal skin substitutes. J Invest Dermatol **137**: 217-227.

Graham GP, Helmer SD, Haan JM, Khandelwal A (2013) The use of Integra® Dermal Regeneration Template in the reconstruction of traumatic degloving injuries. J Burn Care Res **34**: 261-266.

Grässer C, Scheuer C, Parakenings J, Tschernig T, Eglin D, Menger MD, Laschke MW (2016) Effects of macrophage-activating lipopeptide-2 (MALP-2) on the vascularisation of implanted polyurethane scaffolds seeded with microvascular fragments. Eur Cell Mater **32**: 74-86.

Hirche C, Senghaas A, Fischer S, Hollenbeck ST, Kremer T, Kneser U (2016) Novel use of a flowable collagen-glycosaminoglycan matrix (Integra™ Flowable Wound Matrix) combined with percutaneous cannula scar tissue release in treatment of post-burn malfunction of the hand-A preliminary 6 month follow-up. Burns **42**: e1-7.

Junqueira LC, Bignolas G, Brentani RR (1979) Picrosirius staining plus polarization microscopy, a specific method for collagen detection in tissue sections. Histochem J **11**: 447-455.

Killat J, Reimers K, Choi CY, Jahn S, Vogt PM, Radtke C (2013) Cultivation of keratinocytes and fibroblasts in a three-dimensional bovine collagen-elastin matrix (Matriderm®) and application for full thickness wound coverage *in vivo*. Int J Mol Sci **14**: 14460-14474.

Lamme EN, van Leeuwen RT, Jonker A, van Marle J, Middelkoop E (1998) Living skin substitutes: survival and function of fibroblasts seeded in a dermal substitute in experimental wounds. J Invest Dermatol **111**: 989-995.

Laschke MW, Kleer S, Scheuer C, Schuler S, Garcia P, Eglin D, Alini M, Menger MD (2012) Vascularisation of porous scaffolds is improved by incorporation of adipose tissue-derived microvascular fragments. Eur Cell Mater **24**: 266-277.

Laschke MW, Kleer S, Scheuer C, Eglin D, Alini M, Menger MD (2015) Pre-cultivation of adipose tissue-derived microvascular fragments in porous scaffolds does not improve their *in vivo* vascularisation potential. Eur Cell Mater **29**: 190-200.

Laschke MW, Menger MD (2015) Adipose tissue-derived microvascular fragments: natural vascularization units for regenerative medicine. Trends Biotechnol **33**: 442-448.

Laschke MW, Menger MD (2016) The dorsal skinfold chamber: a versatile tool for preclinical research in tissue engineering and regenerative medicine. Eur Cell Mater **32**: 202-215.

MacNeil S (2007) Progress and opportunities for tissue-engineered skin. Nature **445**: 874-880.

McDaniel JS, Pilia M, Ward CL, Pollot BE, Rathbone CR (2014) Characterization and multilineage potential of cells derived from isolated microvascular fragments. J Surg Res **192**: 214-222.

Melendez MM, Martinez RR, Dagum AB, McClain SA, Simon M, Sobanko J, Zimmerman T, Wetterau M, Muller D, Xu X, Singer AJ, Arora B (2008) Porcine wound healing in full-thickness skin defects using Integra™ with and without fibrin glue with keratinocytes. Can J Plast Surg **16**: 147-152.

Meruane MA, Rojas M, Marcelain K (2012) The use of adipose tissue-derived stem cells within a dermal substitute improves skin regeneration by increasing neoangiogenesis and collagen synthesis. Plast Reconstr Surg **130**: 53-63.

Nunes SS, Greer KA, Stiening CM, Chen HY, Kidd KR, Schwartz MA, Sullivan CJ, Rekapally H, Hoying JB (2010) Implanted microvessels progress through distinct neovascularization phenotypes. Microvasc Res **79**: 10-20.

Pirayesh A, Hoeksema H, Richters C, Verbelen J, Monstrey S (2015) Glyaderm® dermal substitute: clinical application and long-term results in 55 patients. Burns **41**: 132-144.

Radhika T, Sekaran P, Narasimhan M (2016) Qualitative analysis of collagen fibers in oral submucous fibrosis using picrosirius reds and polarising microscope. J Clin Diagn Res **10**: ZC04-7.

Reid MJ, Currie LJ, James SE, Sharpe JR (2007) Effect of artificial dermal substitute, cultured keratinocytes and split thickness skin graft on wound contraction. Wound Repair Regen **15**: 889-896.

Rowan MP, Cancio LC, Elster EA, Burmeister DM, Rose LF, Natesan S, Chan RK, Christy RJ, Chung KK (2015) Burn wound healing and treatment: review and advancements. Crit Care **19**: 243.

Ruszczak Z (2003) Effect of collagen matrices on dermal wound healing. Adv Drug Deliv Rev **55**: 1595-1611.

Shahrokhi S, Arno A, Jeschke MG (2014). The use of dermal substitutes in burn surgery: acute phase. Wound Repair Regen **22**: 14-22.

Sorg H, Krueger C, Schulz T, Menger MD, Schmitz F, Vollmar B (2009) Effects of erythropoietin in skin wound healing are dose related. FASEB J **23**: 3049-2058.

Sorg H, Krueger C, Vollmar B (2007) Intravital insights in skin wound healing using the mouse dorsal skin fold chamber. J Anat **211**: 810-818.

Später T, Frueh FS, Metzger W, Menger MD, Laschke MW (2016) *In vivo* biocompatibility, vascularization, and incorporation of Integra® dermal regenerative template and flowable wound matrix. J Biomed Mater Res B Appl Biomater, doi: 10.1002/jbm.b.33813.

Young RG, Butler DL, Weber W, Caplan AI, Gordon SL, Fink DJ (1998) Use of mesenchymal stem cells in a collagen matrix for Achilles tendon repair. J Orthop Res **16**: 406-413.

Zonari A, Martins TM, Paula AC, Boeloni JN, Novikoff S, Marques AP, Correlo VM, Reis RL, Goes AM (2015)

Polyhydroxybutyrate-co-hydroxyvalerate structures loaded with adipose stem cells promote skin healing with reduced scarring. Acta Biomater **7**: 170-181.

Discussion with Reviewers

Daniel Schmauss: From which region of the body would you prefer fat tissue to be obtained, in order to translate your study into a clinical setting?

Authors: In the clinical setting, ad-MVF may be minimal-invasively harvested from a patient by liposuction. Since subcutaneous white fat tissue generally exhibits a good vascularisation, its origin may not be of particular importance. In fact, the body region for the harvesting of fat tissue may even be individually chosen according to the specific needs of the patient. In most cases it may be liposuction of subcutaneous fat from the abdominal wall or thighs.

Norbert Pallua: Results are rather descriptive depending on the used assay. Thus, the overall relevance of findings is limited, since no specific cell line, mechanism/functions or novel aspect related to wound healing are discernible.

Authors: We agree with the reviewer that our results are rather descriptive. However, although we do not provide novel mechanistic insights into the process of wound healing, our results may be highly relevant for the future clinical application of ad-MVF. In fact, based on our results it may be concluded that ad-MVF-seeded FWM may be particularly recommended as an injectable ad-MVF carrier for the minimal-invasive filling of small, hardly accessible defects with an irregular geometry. In contrast, for the coverage of large skin defects, such as caused by extensive burns, ad-MVF-seeded MWD may be more suitable.

Editor's note: The Scientific Editor responsible for this paper was Christopher Evans.